Electron-helium *S*-wave model benchmark calculations. II. Double ionization, single ionization with excitation, and double excitation

Philip L. Bartlett[1,*] and Andris T. Stelbovics[2,†]
[1]*Centre for Antimatter-Matter Studies, Murdoch University, Perth 6150, Australia*
[2]*Centre for Antimatter-Matter Studies, Curtin University, Perth 6102, Australia*
(Received 3 November 2009; published 18 February 2010)

The propagating exterior complex scaling (PECS) method is extended to all four-body processes in electron impact on helium in an *S*-wave model. Total and energy-differential cross sections are presented with benchmark accuracy for double ionization, single ionization with excitation, and double excitation (to autoionizing states) for incident-electron energies from threshold to 500 eV. While the PECS three-body cross sections for this model given in the preceding article [Phys. Rev. A **81**, 022715 (2010)] are in good agreement with other methods, there are considerable discrepancies for these four-body processes. With this model we demonstrate the suitability of the PECS method for the complete solution of the electron-helium system.

DOI: 10.1103/PhysRevA.81.022716 PACS number(s): 34.80.Dp

I. INTRODUCTION

Recent advances in measurement techniques have allowed kinematically complete measurements of the electron-impact double ionization of helium to be made [1,2]. Together with fully differential measurements for the electron-impact single ionization with excitation [3] (where the He^+ ion is left in an excited state), a significant insight has been given into the complex dynamics of the full four-body system. While theoretical methods have provided accurate *ab initio* calculations for the three-body channels open to these collisions, such as convergent close coupling (CCC) [4], *R* matrix with pseudostates (RMPS) [5], and time-dependent close coupling (TDCC) [6], the progress of *ab initio* methods on the four-body channels has been limited. Hybrid methods that combine CCC or RMPS with distorted-wave techniques, or indeed full distorted-wave methods, have made some progress in this regard [1,3] though large discrepancies remain, especially with low-energy collisions. Presently, TDCC is the only *ab initio* method that has been applied to electron-impact double ionization of helium, and while it is in reasonable agreement with measurements of the total cross sections [7], angular-differential calculations differ markedly from measurement [8]. There is, therefore, a growing need for accurate theoretical modeling of four-body processes.

The *S*-wave model for electron-helium collisions retains a single partial wave of the full collision system that has zero angular momentum for all three electrons. This model serves as an ideal test bed for new theoretical methods as it retains all the features of the full system, but requires significantly less computational effort. The *ab initio* methods that have already been applied to this model include TDCS [9], CCC [10], and time-dependent exterior complex scaling (TD-ECS) [11]. Significantly, however, none of these methods has been applied to all three- and four-body processes open to this model, and no energy-differential results have yet been presented for four-body processes.

In the preceding article [12] we described the propagating exterior complex scaling (PECS) four-body method for calculating electron-helium scattering wave functions and presented benchmark excitation and single-ionization (without excitation) cross sections (total and energy-differential) for the *S*-wave model. Here we complete our study of the *S*-wave model. In Sec. II we detail the PECS method for extracting double-ionization cross sections from a scattering wave function, and in Sec. III we present a comprehensive set of benchmark cross sections for electron-impact double ionization, ionization with excitation, and double excitation from ground-state helium targets. To conclude, we present a small sample of double-ionization cross sections for excited-state targets.

II. THEORY

The preceding article [12] detailed the PECS four-body method for calculating the scattering wave functions for electron-helium collisions in the *S*-wave model, along with surface integral methods for evaluating non-breakup and single-ionizing collisions. In summary, this method numerically solves the full time-independent Schrödinger equation for electron-helium on a numerical mesh in coordinate space. The exterior complex scaling (ECS) transformation is applied at a distance R_0 from the nucleus, which rotates the radial coordinates into the complex plane and causes all outgoing waves to be exponentially damped. This allows the outer boundary condition of the mesh to be approximated by zero, and the system of differential equations can be solved without knowledge of the asymptotic form of the scattering wave function. The ECS transformation was successfully applied to ionizing collisions by Rescigno *et al.* [13] using the electron-hydrogen three-body system. The numerical implementation was later enhanced by Bartlett *et al.* [14] by incorporating a highly efficient propagation algorithm and iterative coupling procedure.

In ECS-based methods the cross sections are extracted from the scattering wave function using a surface integral technique [15], which has been demonstrated [14,16] to provide highly accurate ionization and scattering cross sections

*p.bartlett@murdoch.edu.au
†a.stelbovics@curtin.edu.au

for electron-hydrogen collisions. In the preceding article [12], this surface integral technique was used to calculate excitation and single-ionization cross sections for the four-body electron-helium S-wave model. These same equations are used to evaluate the double-excitation and ionization-with-excitation cross sections presented here, simply by using the appropriate final-state atom/ion wave function in Eqs. (26) and (36) of the preceding article [12]. A method for evaluating cross sections for the remaining four-body channel, double ionization is developed here.

A. Double ionization

The equations used to extract the double-ionization amplitude from a scattering wave function are derived in a way similar to that of excitation and single ionization given in the preceding article [12] and we start with an integral formulation for the amplitude presented in Peterkop [15],

$$\boldsymbol{I}^{S}_{ji}(\boldsymbol{k}_0,\boldsymbol{k}_1,\boldsymbol{k}_2) = \int dV\, \boldsymbol{\Psi}_i^{SM_S(+)}(0,1,2)\,(\boldsymbol{H}-E)\,\boldsymbol{\Phi}^{SM_S(-)^*}_{j,\boldsymbol{k}_0,\boldsymbol{k}_1,\boldsymbol{k}_2}(0,1,2), \quad (1)$$

where $\boldsymbol{\Psi}_i^{SM_S(+)}(0,1,2)$ is the antisymmetrized outgoing scattering wave function, S is the total spin angular momentum, M_S is its magnetic substate, and i represents the momentum of the incident electron $\boldsymbol{k}_i$ and the energy ϵ_i and initial state $|l_i m_{l_i} s_i m_{s_i}\rangle$ of the target. The three electrons are represented by a radial and spin part given by $n \equiv (\boldsymbol{r}_n, \sigma_n)$, and as total spin is conserved, they may be decoupled using

$$\boldsymbol{\Psi}_i^{SM_S(+)}(0,1,2) = \sum_{s_{12}} \boldsymbol{\Psi}^{SM_S(+)}_{i,s_{12}}(\boldsymbol{r}_0,\boldsymbol{r}_1,\boldsymbol{r}_2)\chi_{s_{12}SM_S}(\sigma_0,\sigma_1,\sigma_2), \quad (2)$$

where s_{12} is the spin angular momentum of an arbitrary two-electron substate for which electrons 1 and 2 are used throughout these derivations. $\boldsymbol{\Phi}^{SM_S(-)}_{j,\boldsymbol{k}_0,\boldsymbol{k}_1,\boldsymbol{k}_2}$ is an asymptotic approximation for the final-state wave function containing three continuum electrons (noting that for double ionization $j \equiv s_j$). By applying the divergence theorem and normalization constants and using the known relation between this integral and the partial-wave amplitude, ($I = -2\pi F$) [15], the double-ionization amplitude may be evaluated on the surface of a nine-dimensional hypersphere using

$$\begin{aligned}\boldsymbol{F}^{S}_{ji}(\boldsymbol{k}_0,\boldsymbol{k}_1,\boldsymbol{k}_2) \underset{\rho\to\infty}{\sim} & \frac{\rho^2}{2(2\pi)^4}\int d\hat{\boldsymbol{r}}_0 \int d\hat{\boldsymbol{r}}_1 \int d\hat{\boldsymbol{r}}_2 \\ & \times \int_0^{\pi/2} d\alpha \int_0^{\pi/2} d\beta\;\; r_0^2 r_1^2 r_2^2 \cos\beta \\ & \times \left[\boldsymbol{\Phi}^{SM_S(-)^*}_{j,\boldsymbol{k}_0,\boldsymbol{k}_1,\boldsymbol{k}_2}(0,1,2)\frac{\partial}{\partial\rho}\boldsymbol{\Psi}_i^{SM_S(+)}(0,1,2)\right. \\ & \left. - \boldsymbol{\Psi}_i^{SM_S(+)}(0,1,2)\frac{\partial}{\partial\rho}\boldsymbol{\Phi}^{SM_S(-)^*}_{j,\boldsymbol{k}_0,\boldsymbol{k}_1,\boldsymbol{k}_2}(0,1,2)\right]. \end{aligned} \quad (3)$$

The relationships between Cartesian and nine-dimensional hyperspherical coordinates are

$$r_0 = \rho\sin\alpha\cos\beta, \quad (4)$$

$$r_1 = \rho\cos\alpha\cos\beta, \quad (5)$$

$$r_2 = \rho\sin\beta, \quad (6)$$

$$\rho = \sqrt{r_0^2 + r_1^2 + r_2^2}, \quad (7)$$

$$\begin{aligned} d\boldsymbol{S} &= \rho^8 \sin^2\alpha\cos^2\alpha\sin^2\beta\cos^5\beta\; d\alpha d\beta\, d\hat{\boldsymbol{r}}_0 d\hat{\boldsymbol{r}}_1 d\hat{\boldsymbol{r}}_2 \\ &= \rho^2 r_0^2 r_1^2 r_2^2 \cos\beta\; d\alpha d\beta\, d\hat{\boldsymbol{r}}_0 d\hat{\boldsymbol{r}}_1 d\hat{\boldsymbol{r}}_2, \end{aligned} \quad (8)$$

and the antisymmetrized final-state asymptotic wave function is approximated with

$$\begin{aligned}\boldsymbol{\Phi}^{SM_S(-)}_{j,\boldsymbol{k}_0,\boldsymbol{k}_1,\boldsymbol{k}_2}(0,1,2) \sim\; & \mathcal{A}\boldsymbol{\Phi}^{(-)}_{\boldsymbol{k}_0}(\boldsymbol{r}_0)\boldsymbol{\Phi}^{(-)}_{\boldsymbol{k}_1}(\boldsymbol{r}_1)\boldsymbol{\Phi}^{(-)}_{\boldsymbol{k}_2}(\boldsymbol{r}_2) \\ & \times \chi_{s_j SM_S}(0,1,2), \end{aligned} \quad (9)$$

where for a neutral helium target we choose $Z = 2$ Coulomb waves for the continuum waves.

After incorporating partial-wave expansions of the scattering wave function and final-state asymptotic approximation (see [12]) and simplifying for the S-wave model, the partial-wave amplitude for double ionization becomes

$$\begin{aligned} F^{S}_{ji}(k_0,k_1,k_2) \underset{\rho\to\infty}{\sim} & \frac{2\sqrt{6}\rho^2}{\pi k_0 k_1 k_2}\int_0^{\pi/4} d\alpha \int_0^{\theta_\beta} d\beta\;\cos\beta \sum_{s_{12}} \\ & \times \left[\phi^{SM_S(-)}_{j,s_{12},k_0,k_1,k_2}(r_0,r_1,r_2)\frac{\partial}{\partial\rho}\tilde{\psi}^{SM_S}_{i,s_j}\right. \\ & \times (r_0,r_1,r_2) - \tilde{\psi}^{SM_S}_{i,s_j}(r_0,r_1,r_2) \\ & \left. \times \frac{\partial}{\partial\rho}\phi^{SM_S(-)}_{j,s_{12},k_0,k_1,k_2}(r_0,r_1,r_2)\right], \end{aligned} \quad (10)$$

where $\theta_\beta = \arctan(\sin\alpha)$ and

$$\begin{aligned} & \phi^{SM_S(-)}_{j,s_{12},k_0,k_1,k_2}(r_0,r_1,r_2) \\ & = \phi^{(-)}_{k_0}(r_0)[\phi^{(-)}_{k_1}(r_1)\phi^{(-)}_{k_2}(r_2) + (-1)^{s_j}\phi^{(-)}_{k_1}(r_2)\phi^{(-)}_{k_2}(r_1)] \\ & \times \delta s_j s_{12} - \alpha_{01}^{s_j s_{12} S}\phi^{(-)}_{k_0}(r_1)[\phi^{(-)}_{k_1}(r_0)\phi^{(-)}_{k_2}(r_2) + (-1)^{s_j} \\ & \times \phi^{(-)}_{k_1}(r_2)\phi^{(-)}_{k_2}(r_0)] - \alpha_{02}^{s_j s_{12} S}\phi^{(-)}_{k_0}(r_2)[\phi^{(-)}_{k_1}(r_1)\phi^{(-)}_{k_2}(r_0) \\ & + (-1)^{s_j}\phi^{(-)}_{k_1}(r_0)\phi^{(-)}_{k_2}(r_1)]. \end{aligned} \quad (11)$$

The antisymmetrization constants ($\alpha_{0n}^{s_j s_{12} S}$) are given in the Appendix of the preceding article [12]. As both the scattering and asymptotic final-state wave functions are antisymmetric with respect to exchange of electrons, through symmetry arguments Eq. (10) can be evaluated on 1/6 of the hyperspherical surface and a factor of 6 can be included to compensate.

The $Z = 2$ Coulomb waves used for the asymptotic final-state approximation in (11) are orthogonal to the ground and excited states of He^+. In the asymptotic limit of ρ, this ensures that the single-ionization channels (in their asymptotic form of the product of a He^+ wave function and two continuum waves) do not contribute to the double-ionization amplitude calculated on the hyperspherical surface. For practical calculations, convergence studies are undertaken to ensure that a sufficiently large ρ is used to ensure that this asymptotic case is approximated. The $Z = 2$ Coulomb waves are not, however, orthogonal to the helium ground- or excited-state channels. To ensure that these non-breakup channels do not interfere with the double-ionization amplitude an asymptotic subtraction method is used. This method was used in the TD-ECS implementation of this model [11] and also for the single ionization detailed in the preceding article [12]. In

this method, asymptotic approximations of the non-breakup channels are subtracted from the scattering wave function using

$$\tilde{\psi}^{SM_S}_{i,s_{12}}(r_0,r_1,r_2) = \psi^{SM_S}_{i,s_{12}}(r_0,r_1,r_2) - \frac{1}{\sqrt{3}}\sum_{j'}^{j'_{\max}} F^S_{j'i}\left[\delta_{s_{j's_{12}}} e^{ik_{j'}r_0}\phi_{j'}(r_1,r_2) - \alpha^{s_{j's_{12}}S}_{01} e^{ik_{j'}r_1}\phi_{j'}(r_0,r_2) - \alpha^{s_{j's_{12}}S}_{02} e^{ik_{j'}r_2}\phi_{j'}(r_1,r_0)\right], \quad (12)$$

where j' represents a final-state channel with partial-wave amplitude $F^S_{j'i}$, $s_{j'}$ is the final-state spin of the target, and $k_{j'}$ is the momentum of the scattered electron in this channel. The single- and double-ionization calculations presented in this article subtract the $1sns$ singlet and triplet states of helium with $n \leqslant n_{\max} = 3$.

The double-energy-differential double-ionization cross section is calculated using

$$\frac{d^2\sigma_i^S(k_0,k_1,k_2)}{d\epsilon_a d\epsilon_b} = \frac{2S+1}{2(2s_i+1)}\frac{k_0k_1k_2}{k_i}\sum_{s_j}|F^S_{ji}(k_0,k_1,k_2)|^2, \quad (13)$$

where the first term is the spin weighting factor and ϵ_a and ϵ_b are energies of any two of the three continuum electrons with energies ϵ_0, ϵ_1, and ϵ_2. The fast, intermediate, and slow electrons are arbitrarily assigned to labels 0, 1, and 2, respectively. Therefore, the electron energies satisfy the relations

$$0 \leqslant \epsilon_2 \leqslant \epsilon_1 \leqslant \epsilon_0 \leqslant E, \quad (14)$$

$$\epsilon_0 + \epsilon_1 + \epsilon_2 = E. \quad (15)$$

As the double-energy-differential cross section has sixfold symmetry, the total double-ionization cross section can be evaluated by integrating any one of the six regions shown in Fig. 1 by using

$$\sigma_i^S = \int_{\epsilon_a^{\text{lower}}}^{\epsilon_a^{\text{upper}}} d\epsilon_a \int_{\epsilon_b^{\text{lower}}}^{\epsilon_b^{\text{upper}}} d\epsilon_b \frac{d^2\sigma_i^S(k_0,k_1,k_2)}{d\epsilon_a d\epsilon_b}, \quad (16)$$

where Table I gives the limits of integration for the three shaded regions shown in Fig. 1, that have the slow-, intermediate-, or fast-electron energy in the outer integration (ϵ_a).

In order to describe the energy distribution of a single electron scattered or ejected during an electron-helium collision it is necessary to consider the slow, intermediate, *and* fast electrons. The double-energy-differential cross section

TABLE I. Integration limits for total double-ionization cross sections for different energy classifications of the outer integration (ϵ_a). These limits are used in Eq. (16).

Electron a energy	Integration limits			
	$\epsilon_a^{\text{lower}}$	$\epsilon_a^{\text{upper}}$	$\epsilon_b^{\text{lower}}$	$\epsilon_b^{\text{upper}}$
Slow	0	$E/3$	ϵ_a	$(E-\epsilon_a)/2$
Intermediate	0	$E/2$	0	$\min(\epsilon_a, E-2\epsilon_a)$
Fast	$E/3$	E	$\max(E-2\epsilon_a, 0)$	$(E-\epsilon_a)/2$

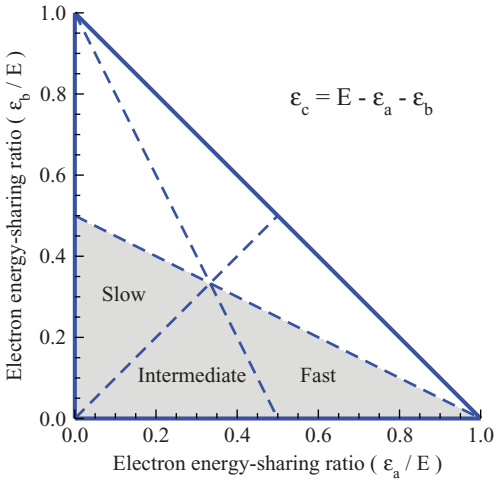

FIG. 1. (Color online) Electron energy-sharing lines of symmetry (dashed lines) and energy integration regions (shaded) for total and single-energy-differential double-ionization cross sections (see text for details).

given in Eq. (13) is integrated over ϵ_b in the entire shaded region shown in Fig. 1, which represents all three energy classifications of the outgoing electrons. However, because the electrons are identical this result is divided by three to give the energy distribution of a single randomly detected electron as

$$\frac{d\,\sigma_i^S(k_0,k_1,k_2)}{d\epsilon_a} = \frac{1}{3}\int_0^{(E-\epsilon_a)/2}\frac{d^2\,\sigma_i^S(k_0,k_1,k_2)}{d\epsilon_a d\epsilon_b}d\epsilon_b. \quad (17)$$

The $1/3$ contribution from the slow, intermediate, and fast electrons to this cross section are shown separately in the results section (Fig. 4). Integrating the single differential cross section (SDCS) as defined in Eq. (14) over the interval $0 \leqslant \epsilon_a \leqslant E$ gives the total cross section, equivalent to Eq. (16).

B. Cross-section convergence

ECS-based methods are capable of highly accurate solutions of the scattering wave function over *all* real regions of their numerical mesh. Investigating the radial convergence of cross sections extracted from the scattering wave function gives a first-order estimate, as a function of ρ, of the error introduced by using an asymptotic approximation for the final-state wave function at finite ρ. This is generally the largest contribution to the error of ECS-based calculations and diminishes with increasing hyperradii. The rate of convergence varies depending on the incident electron energy (E_0), initial state, and final state. Cross sections at energies below the peak cross section and cross sections for higher excitation levels (of the final or initial state) are usually slower to converge and require larger ρ.

The radial convergence of all four-body processes open to the S-wave model at 150 eV are shown in Fig. 2. This energy is well below the peak in the double-ionization cross sections (≈300 eV), below the peaks in the ionization-with-excitation cross section (≈200 eV), and just above the peak in the double-excitation cross sections (≈120 eV). As such,

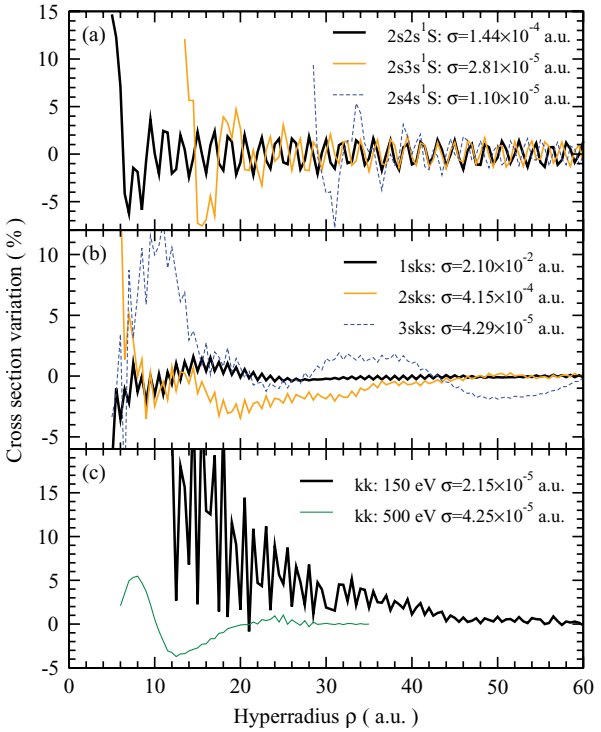

FIG. 2. (Color online) Convergence of cross sections w.r.t. the hyperradius (ρ) for four-body channels from a ground-state target. Results, expressed as a percentage variation from the $\rho \approx 60$ a.u. calculations, are presented for (a) double excitation at $E_0 = 150$ eV, (b) single ionization with excitation at $E_0 = 150$ eV, and (c) double ionization at $E_0 = 150$ eV and $E_0 = 500$ eV. The converged cross sections are given in the legend.

it highlights the radial convergence behavior in a relatively difficult-to-converge energy region. At this energy, relatively good convergence of all but the $4s2s^1S$ final state is obtained near $\rho = 25$ a.u. At 150 eV the double ionization cross section requires a 40 a.u. mesh to converge to benchmark quality, whereas at 500 eV this reduces to below 20 a.u.

The most difficult four-body channels to converge are ionization with excitation. The $\pm 2\%$ long-wavelength oscillation in the cross sections of the $3sks$ channel in Fig. 2 suggests that the helium static continuum waves used for the final-state asymptotic approximation are not ideal. This is discussed in more detail later. Nevertheless, we believe that all of the calculations presented have been undertaken with sufficiently large R_0 (and sufficiently small mesh spacing) to be considered of benchmark quality. The standard error for double excitation and ionization with excitation is estimated to be $(n_j + 1)\%$ (with respect to the peak cross section, where n_j is the orbital quantum number of the final-state atom or ion), and better than 4% for double ionization of a ground-state target. It is worth noting that for this model the cross sections for four-body processes are up to 4 orders of magnitude smaller than the elastic cross section (0.71 a.u.) at 150 eV and up to 3 orders of magnitude smaller than single ionization ($1sks$).

The convergence of the double-ionization cross section with respect to (w.r.t.) the number of non-breakup channels ($n_{\max}$) that are asymptotically subtracted from the scattering wave function is shown in Fig. 3. Clearly, the elastic

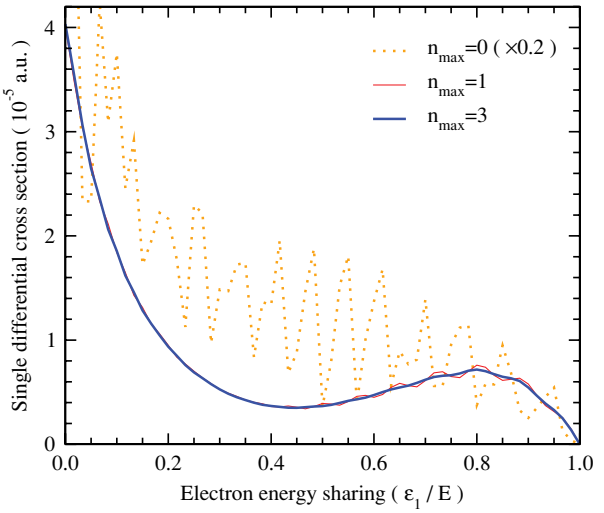

FIG. 3. (Color online) Convergence of single-energy-differential double-ionization cross sections w.r.t. the number of excitation channels subtracted from the scattering wave function ($n_{\max}$) for a ground-state target with $E_0 = 150$ eV.

channel is a significant cause of interference, but subtracting higher excitation channels has minimal effect due to their approximate orthogonality with the $Z = 2$ Coulomb waves used with the double-ionization channels. At $n_{\max} = 3$ the single-energy-differential cross section is remarkably smooth and gives strong support for the efficacy of this subtraction method with double ionization.

III. RESULTS

A. Double ionization

The single and double (DDCS) energy-differential cross sections for double ionization in the S-wave model are presented in Fig. 4 at $E_0 = 150$, 300, and 500 eV. Energy-differential cross section results for double ionization in this model have not previously been published so only empirical observations can be made. These results are distinguished by several significant features: The cross sections are 100 times smaller than single ionization; the DDCSs have pronounced peaks when the energies of two of the outgoing (ejected) electrons are small (i.e., the scattered electron retains the bulk of the system energy); the SDCS is dominated by low-energy electrons; the base of the DDCS becomes flatter (with steeper slopes) as the system energy increases, and the calculations are remarkably smooth at all energies. It should be noted that in this S-wave model, where all angular momenta are zero, that $\Psi_i^{SM_S}(r_0, r_1, r_2) = 0$ along the vector $r_0 = r_1 = r_2$. This is due to the fact that at any time at least two of the electrons have spins in the same direction and so cannot occupy the same space coordinate due to the Pauli exclusion principle. Consequently, in the asymptotic region where the double-ionization amplitude dominates, the momenta of the electrons is determined by their classical trajectories and the ratio of the momenta is the same as the ratio of the space coordinates. Hence the DDCS is necessarily zero when $\epsilon_1 = \epsilon_2 = \epsilon_3$. This is clearly evident in the double differential cross sections of Fig. 4, and the zero vector is discernible in

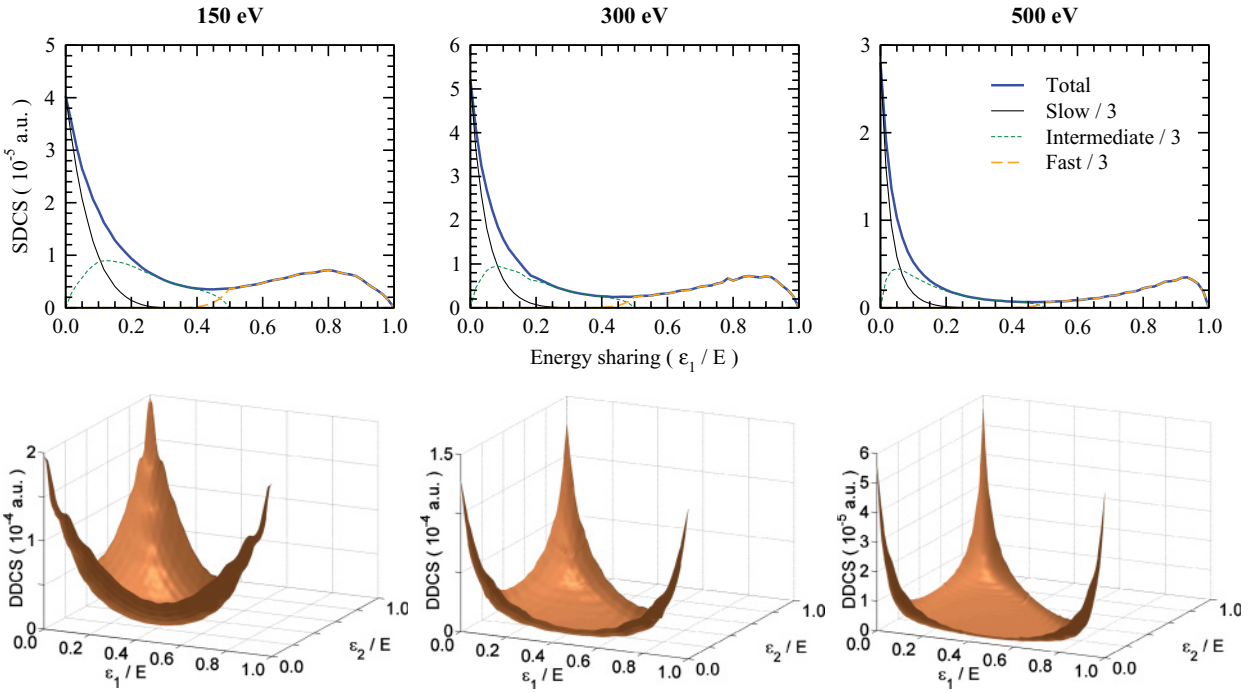

FIG. 4. (Color online) Single-energy-differential (top) and double-energy-differential (bottom) cross sections for double ionization of ground-state helium by 150-, 300-, and 500-eV incident electrons.

the wave function plots shown in Fig. 3 of the preceding article [12]. This restriction is not imposed on other partial waves, so these S-wave results do not apply to the full electron-helium system unless we have the additional condition that the space directions of the three electrons are identical.

At 150 eV the total cross section for double ionization has only reached approximately 1/3 of its peak value (at ≈300 eV), so this energy can be considered to be close to the near-threshold region, which generally requires significantly larger ρ and is notoriously difficult to obtain well-converged results.

The total double-ionization cross sections are shown in Fig. 5 from threshold to 500 eV, along with the ratio of single to double ionization. These results are compared with the TDCC S-wave calculations of Pindzola *et al.* [9] and measurements of the real e-He system by Shah *et al.* [17] (normalized to the present results at 275 eV). It is clear that the energy dependence of the S-wave double-ionization cross section differs significantly from the real system, especially near threshold. The S-wave results are significantly suppressed for about 40 eV above the threshold energy (78.3 eV). This is reminiscent of the near-threshold suppression of the single-ionization cross sections of the equivalent S-wave model for electron-hydrogen [18], though over a much larger energy range here.

The TDCC results for total double ionization are approximately 2.6 times larger than the present results. While this is a significant variation, the TDCC results were not converged w.r.t. mesh spacing. The TDCC article [9] presents a convergence study for excitation and ionization of e-He^+ so as to estimate the possible error introduced by their overly large grid spacing. At the same grid spacing as their e-He calculations the results for this simpler three-body system are overstated by a factor of approximately 1.8. Given the nonconvergence of the TDCC results, we believe that they can only provide an order-of-magnitude check of the present fully converged calculations. No S-wave double-ionization results have been published for the TD-ECS or CCC methods.

In [9], the authors noted that while the individual TDCC cross sections were not converged w.r.t. grid spacing, the ratio of single ionization to double ionization appeared to be better converged. Two sets of TDCC results are presented on the single/double ionization ratio plot in Fig. 5, obtained from single-ionization calculations that used charges of $Z = 1$ and $Z = 2$ for the final-state continuum waves. Asymptotically, we would expect that $Z = 1$ is the optimal choice for single ionization of a neutral target. There is good agreement between the PECS ionization ratio and TDCC at 300 eV and above, which supports their choice of $Z = 1$ for the single-ionization continuum waves.

While there is no *a priori* reason to expect the single-ionization/double-ionization ratios for the S-wave model to be consistent with measurements of the real system, we do believe they are a check of the reasonableness of our calculations. The ratio of the S-wave model is significantly higher at low energies, but this is readily accounted for by the suppression of the double-ionization cross section near threshold in the S-wave model. At high energies the S-wave results are mostly within a factor of 2 of measurement.

B. Single ionization with excitation

Figure 6 shows total single-ionization cross section calculations with ($2sks$, $3sks$) and without ($1sks$) excitation of the final-state He^+ ion, from threshold to 500 eV. Our PECS calculations for the $1sks$ three-body channel from the preceding article [12] are repeated here and are in excellent

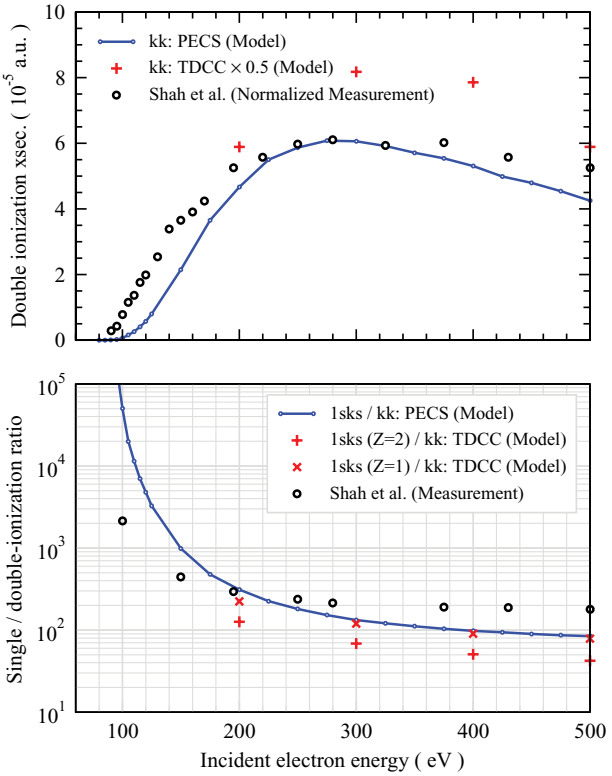

FIG. 5. (Color online) Double ionization of a ground-state target by 80- to 500-eV incident electrons: (a) total cross section and (b) ratio of single-ionization cross section (without excitation) divided by double-ionization cross section. TDCC model calculations [9] and measurements [17] of the full e-He system are included for comparison.

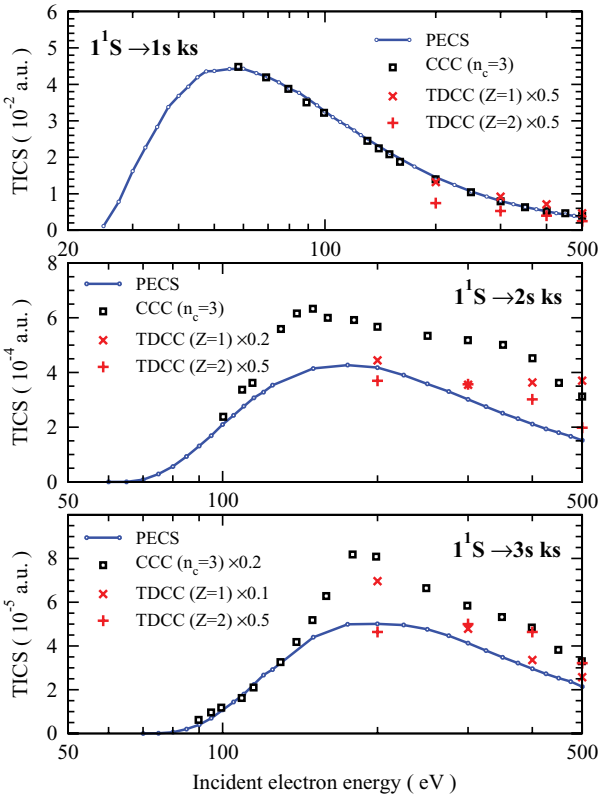

FIG. 6. (Color online) Total cross sections for electron-impact single ionization without ($1sks$) and with ($2sks$, $3sks$) excitation of the final-state He^+ ion for $E_0 = 24$–500 eV from a ground-state target. CCC [19] ($n_c = 3$) and TDCC [9] calculations are included for comparison.

agreement with results from CCC [19] and TD-ECS [11] (not shown here) over a wide range of energies. The close agreement of these three methods for the $1sks$ final state confirms that all three methods for single ionization from the ground state, leaving the core electron in the ground He^+ state, describe this essentially three-body process adequately. Both PECS and TD-ECS use $Z = 1$ continuum waves in their final-state asymptotic approximations, as the bound electron of He^+ shields the $Z = 2$ core. While the TDCC ($Z = 2$) results [9] are in close agreement with PECS (before our $\times 0.5$ scaling of their results), we believe the that the TDCC ($Z = 1$) results are the preferred results to use for comparison because the TDCC single-ionization/double-ionization ratio is in reasonable agreement with PECS when their $Z = 1$ single-ionization results are used (see Fig. 5) and because the nonconvergence of the TDCC grids may account for an overstatement of their results by a factor of 1.8 (see discussion in previous section). Consequently, the TDCC calculations have been scaled by 0.5 in Fig. 6 and reasonable agreement is obtained with PECS and CCC results at 200 eV, though the TDCC results do not diminish as quickly as PECS or CCC calculations at higher energies.

The PECS calculations for all single-ionization processes presented in Fig. 6 have a very smooth energy dependence. This, combined with our convergence studies, supports our claim of benchmark accuracy for these calculations. However, the CCC and TDCC calculations for the ionization-with-excitation channels are not in agreement. The CCC results for $2sks$ exhibit a fair amount of scatter and are approximately 50% higher than PECS at 200 eV, increasing to 100% higher at 500 eV. For the $3sks$ channel, the CCC results are around six times larger than the PECS calculations. In an attempt to investigate the reasonableness of these results it is useful to compare the falloff of the single-ionization results (w.r.t. increasing excitation of the final-state ion) with the falloff of the single-excitation results (where PECS and CCC are in agreement [12]). At 200 eV, the single-ionization ratio ($1sks : 2sks : 3sks$) for PECS is ($1 : 0.029 : 0.0035$) versus ($1 : 0.041 : 0.029$) for CCC, and the ratios for the singlet single-excitation cross sections ($1s1s : 1s2s : 1s3s$) at this energy are ($1 : 0.017 : 0.0042$). We see that the PECS single-ionization calculations have a falloff similar to that of the single-excitation channels, which suggests that the CCC $3sks$ calculations may be overstated. This, combined with the minimum core basis functions ($n_c = 3$) used for the CCC calculations, leads us to conclude that the CCC $3sks$ calculations are not converged.

The TDCC results for ionization with excitation on the other hand are in marked disagreement with the PECS calculations as well as with the CCC calculations. Given that neither the CCC calculations nor the TDCC calculations have demonstrated convergence, in contrast with the present PECS calculations, it is not useful to undertake further comparisons with these ionization-with-excitation results.

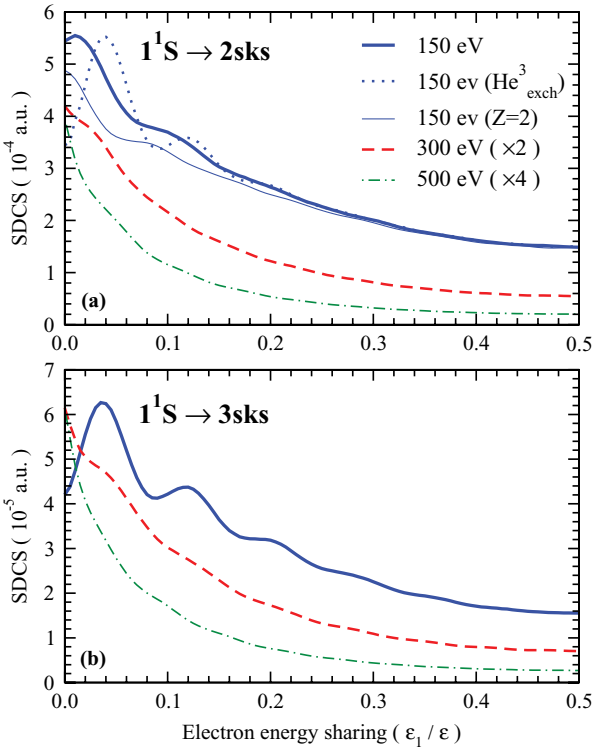

FIG. 7. (Color online) Single-energy-differential cross sections for electron-impact single excitation with excitation from a ground-state helium target in the S-wave model for $E_0 = 150$, 300, and 500 eV. Calculations used helium static continuum waves, except $2sks$ at 150 eV where calculations using helium triplet static exchange (He^3_{exch}) and $Z = 2$ Coulomb continuum waves are also shown.

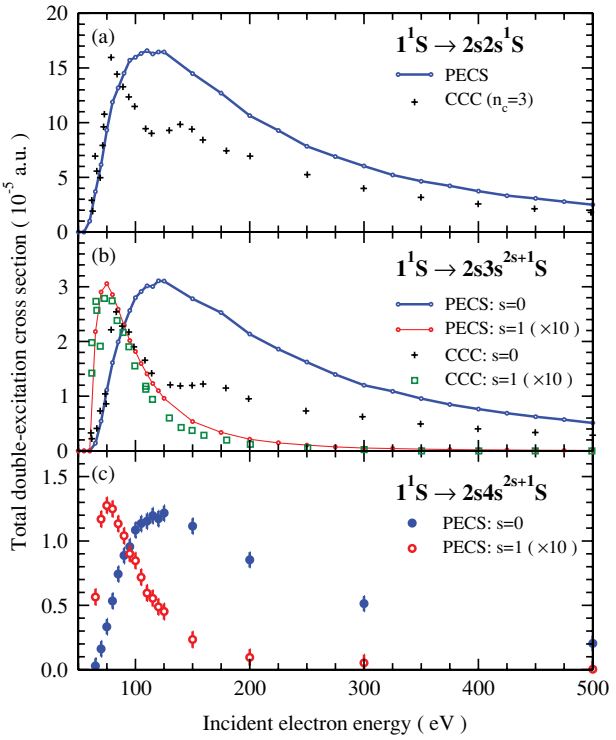

FIG. 8. (Color online) Total cross sections for electron-impact double excitation of a ground-state helium target with $E_0 = 50$–500 eV. CCC calculations [19] are included for comparison. See text for discussion of $2s4s$ convergence.

One feature of the TDCC calculations that we have investigated further is the use of $Z = 2$ continuum waves. In Fig. 7 we present the SDCSs for ionization with excitation at $E_0 = 150$, 300, and 500 eV. Near equal-energy sharing at 150 eV for the $2sks$ final state there is no difference between our calculations undertaken with $Z = 2$ Coulomb waves, $Z = 1$ helium triplet static exchange continuum waves, or $Z = 1$ helium static continuum waves (see the preceding article [12] for a discussion on these different continuum waves). Only at highly asymmetric energy-sharing is there any significant variation. A full-convergence study for single ionization (with and without excitation) was undertaken using each of these continuum waves. The maximum difference between the converged cross sections of the $Z = 1$ continuum waves was around 1%, whereas the $Z = 2$ cross sections were understated by around 5%, though not fully converged w.r.t. the hyperradius. At very large hyperradii, we expect that the $Z = 2$ results will converge with the $Z = 1$ calculations. This 5% difference between $Z = 1$ and $Z = 2$ continuum wave calculations contrasts markedly with the 200–500% difference exhibited by the TDCC results.

While there are minor oscillations in the lower-energy $2sks$ SDCS calculations, which increase in magnitude in the $3sks$ calculations, the integrated cross sections remain well converged. These oscillations are similar to those seen in the $1sks$ SDCS at very low energies (see Fig. 9 in [12]) and are seen to diminish with increasing hyperradius and with increasing energy. No other energy-differential calculations for ionization with excitation are available for comparison.

C. Double excitation

The final four-body channels open to the S-wave model are short-lifetime double-excitation states that lead to autoionization. In the preceding article [12] the interference of these channels with the single ionization of excited-state targets could be seen in the total and energy-differential single-ionization cross sections. PECS results for excitation of the ground state to the $2s2s^1S$, $2s3s^1S$, $2s3s^3S$, $2s4s^1S$, and $2s4s^3S$ doubly excited states are shown in Fig. 8. While there is reasonable agreement with CCC calculations [19], for $2s3s^3S$, there is only general agreement with the cross section maxima, but not shape, for the $2s2s^1$ and $2s3s^1S$ singlet channels. The CCC single calculations show local minima near 125 eV that are not evident in the PECS calculations. Double-excitation calculations for other methods have not been published for this model.

The discrepancy between the PECS and CCC calculations is attributed to the CCC calculations using a real-only Laguerre basis for the helium doubly excited wave functions. Our investigation of this method found that convergent (real) energies for the singlet doubly excited states of helium could not be obtained with a real-only Laguerre basis, regardless of the basis size. In the preceding article [12] we gave details of our complex-energy method for evaluating the helium doubly excited states and we gave converged complex energies for the first few states. The imaginary part of the energy of these

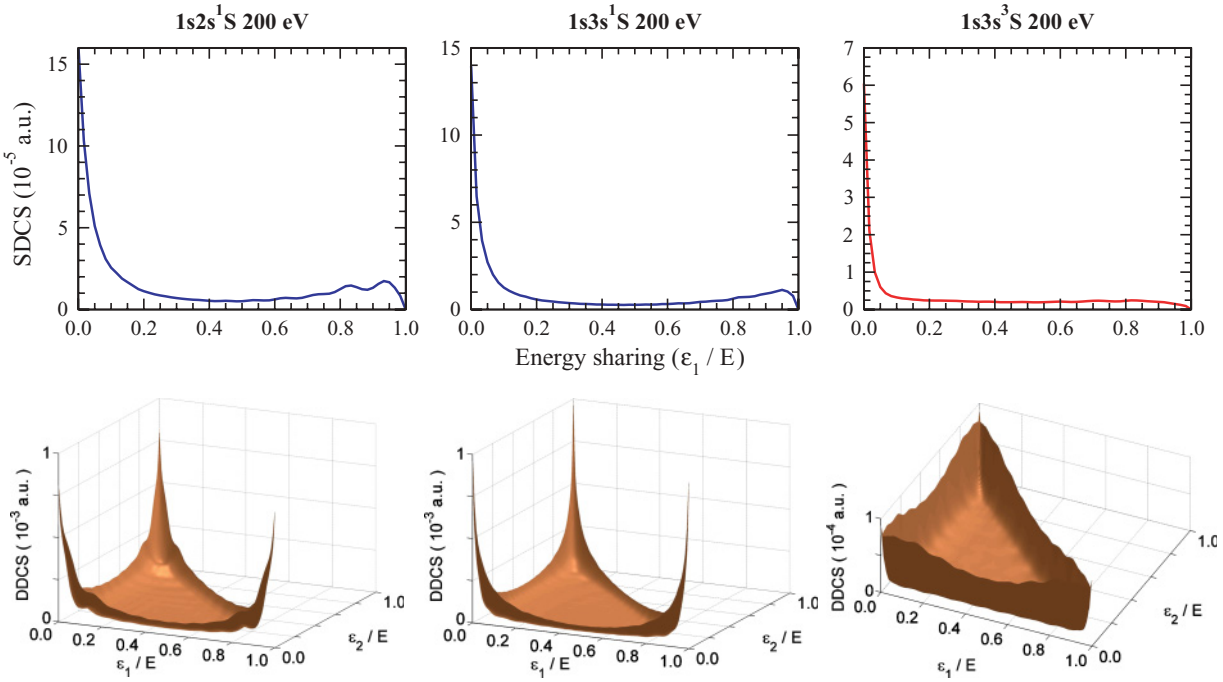

FIG. 9. (Color online) Single-energy-differential (top) and double-energy-differential (bottom) cross sections for double ionization of $1s2s^1S$, $1s3s^1S$, and $1s3s^3S$ (left to right) excited-state helium targets by 200-eV incident electrons.

states is inversely proportional to the lifetime of the state. In our study of the double-excitation channels we trialed using a real Laguerre basis for the helium final-state wave functions in our PECS double-excitation calculations and could not obtain convergence (w.r.t. the hyperradius of the surface integral) or smooth total cross sections (w.r.t. E_0). The triplet double-excited states of helium, however, have a very small imaginary part (long lifetime) and the real-only Laguerre basis is able to give a good approximation of these triplet wave functions. Consequently, the $2s3s^3S$ PECS and CCC calculations are in much better agreement.

The convergence study of the $2s4s^1S$ double-excitation cross section shown in Fig. 2(a) suggests that ρ larger than 45 a.u. are required in order to obtain benchmark quality results. Many of our high-energy calculations were undertaken with a mesh smaller than 45 a.u. and have been removed from the $2s4s$ plots, while many of the remaining calculations were not undertaken with a mesh significantly larger than this for us to be confident of the accuracy of our $2s4s$ calculations. We present these calculations with 5% error bars to indicate their possible error, but do not claim benchmark status.

D. Excited-state targets

So far we have focused on four-body excitation and ionization processes for ground-state targets. To demonstrate that the PECS method can evaluate well-converged four-body cross sections for excited targets we present SDCSs and DDCSs for several excited-state targets at 200 eV in Fig. 9. Comparing the singlet DDCSs in this figure with those of the ground state in Fig. 4, we see that the DDCSs become increasingly flatter in the central region, with increasingly steeper peaks as the orbital quantum number ($1sns$) of the target increases. This trend parallels that exhibited for increasing E_0 shown in Fig. 4.

Figure 9 also shows markedly different energy-sharing behavior for the $1s3s^3S$ triplet target. For singlet targets, the DDCS is largest when the energy of two of the continuum electrons is small. For $1s3s^3S$ the DDCS is largest when the energy of one electron is small, with the energy sharing of the remaining two electrons having little influence on the cross section. For example, for a $E = 100$ eV collision, the probability of the three continuum electrons having energies of 2, 49, and 49 eV is similar to that for 2, 2, and 96 eV continuum electrons. This behavior is representative of all other triplet targets examined, but it is not known if this is an unphysical artifact of the S-wave model.

IV. CONCLUSION

In this article we have provided a comprehensive study of the total and energy-differential cross sections for all four-body processes open to the electron-helium system in the S-wave model. The convergence studies presented support the benchmark claim attributed to the PECS calculations, and the results highlight significant discrepancies with earlier CCC [19] and TDCC [9] calculations for these four-body processes. In combination with the results for three-body processes presented in the preceding article [12], the four-body PECS method has been demonstrated to be able to compute accurate cross sections for all processes open to the electron-helium system over a wide range of energies.

The four-body PECS method developed in the preceding article [12] and this article will now be extended to the full electron-helium problem. The iterative coupling procedures developed for the three-body implementation of PECS [14,20]

will be incorporated into the four-body algorithms, which should minimize the computational overhead required to couple the large number of partial waves that are likely to be required to give converged results for the full problem, especially at high energies.

ACKNOWLEDGMENTS

We acknowledge the Australian Research Council for funding this research and the National Computational Infrastructure Facility for providing supercomputing facilities.

[1] M. Dürr, A. Dorn, J. Ullrich, S. P. Cao, A. Czasch, A. S. Kheifets, J. R. Götz, and J. S. Briggs, Phys. Rev. Lett. **98**, 193201 (2007).
[2] X. Ren, A. Dorn, and J. Ullrich, Phys. Rev. Lett. **101**, 093201 (2008).
[3] S. Bellm, J. Lower, and K. Bartschat, Phys. Rev. Lett. **96**, 223201 (2006).
[4] D. V. Fursa and I. Bray, Phys. Rev. A **52**, 1279 (1995).
[5] K. Bartschat, E. T. Hudson, M. P. Scott, P. G. Burke, and V. M. Burke, Phys. Rev. A **54**, R998 (1996).
[6] M. S. Pindzola and F. J. Robicheaux, Phys. Rev. A **61**, 052707 (2000).
[7] M. S. Pindzola, F. J. Robicheaux, J. P. Colgan, M. C. Witthoeft, and J. A. Ludlow, Phys. Rev. A **70**, 032705 (2004).
[8] M. S. Pindzola, F. Robicheaux, and J. P. Colgan, J. Phys. B **41**, 235202 (2008).
[9] M. S. Pindzola, D. Mitnik, and F. Robicheaux, Phys. Rev. A **59**, 4390 (1999).
[10] C. Plottke, I. Bray, D. V. Fursa, and A. T. Stelbovics, Phys. Rev. A **65**, 032701 (2002).
[11] D. A. Horner, C. W. McCurdy, and T. N. Rescigno, Phys. Rev. A **71**, 012701 (2005).
[12] P. L. Bartlett and A. T. Stelbovics, Phys. Rev. A **81**, 022715 (2010).
[13] T. N. Rescigno, M. Baertschy, W. A. Isaacs, and C. W. McCurdy, Science **286**, 2474 (1999).
[14] P. L. Bartlett, A. T. Stelbovics, and I. Bray, J. Phys. B **37**, L69 (2004).
[15] R. K. Peterkop, *Theory of Ionization of Atoms by Electron Impact* (Colorado Associated University Press, Boulder, CO, 1977).
[16] M. Baertschy, T. N. Rescigno, and C. W. McCurdy, Phys. Rev. A **64**, 022709 (2001).
[17] M. B. Shah, D. S. Elliott, P. McCallion, and H. B. Gilbody, J. Phys. B **21**, 2751 (1988).
[18] P. L. Bartlett and A. T. Stelbovics, Phys. Rev. A **69**, 022703 (2004).
[19] C. Plottke, P. Nicol, I. Bray, D. V. Fursa, and A. T. Stelbovics, J. Phys. B **37**, 3711 (2004).
[20] P. L. Bartlett, J. Phys. B **39**, R379 (2006).